The quantum needle of the avian magnetic compass

Hamish G. Hiscock, Susannah Worster, Daniel R. Kattnig, Charlotte Steers, Ye Jin, David E. Manolopoulos, Henrik Mouritsen and P. J. Hore*

* To whom correspondence may be addressed: peter.hore@chem.ox.ac.uk

Supporting Information

S1. Hyperfine interactions and relative orientation of $FAD^{\bullet-}$ *and* $TrpH^{\bullet+}$

Table S1. Hyperfine tensors for the $FAD^{\bullet-}$ radical.♥

Nucleus	A	a_{iso}/mT♦	T_{qq}/mT ♣
N5	$\begin{pmatrix} -0.0989 & 0.0039 & 0.0 \\ 0.0039 & -0.0881 & 0.0 \\ 0.0 & 0.0 & 1.7569 \end{pmatrix}$	0.5233	1.2336 –0.6101 –0.6234
N10	$\begin{pmatrix} -0.0190 & -0.0048 & 0.0 \\ -0.0048 & -0.0196 & 0.0 \\ 0.0 & 0.0 & 0.6046 \end{pmatrix}$	0.1887	0.4159 –0.2031 –0.2128
H6	$\begin{pmatrix} -0.2569 & -0.1273 & 0.0 \\ -0.1273 & -0.4711 & 0.0 \\ 0.0 & 0.0 & -0.4336 \end{pmatrix}$	–0.3872	0.1896 –0.0464 –0.1432
H8 (×3)	$\begin{pmatrix} 0.4399 & 0.0 & 0.0 \\ 0.0 & 0.4399 & 0.0 \\ 0.0 & 0.0 & 0.4399 \end{pmatrix}$	0.4399	0.0 0.0 0.0
Hβ (×2)	$\begin{pmatrix} 0.4070 & 0.0 & 0.0 \\ 0.0 & 0.4070 & 0.0 \\ 0.0 & 0.0 & 0.4070 \end{pmatrix}$	0.4070	0.0 0.0 0.0
H7 (×3)	$\begin{pmatrix} -0.1416 & 0.0 & 0.0 \\ 0.0 & -0.1416 & 0.0 \\ 0.0 & 0.0 & -0.1416 \end{pmatrix}$	–0.1416	0.0 0.0 0.0

♥Calculated by Dr Ilya Kuprov, Department of Chemistry, University of Southampton using density functional theory in Gaussian-03 (1) at the UB3LYP/EPR-III level (2). The calculation was done for the radical anion of 7,8,10-trimethyl isoalloxazine (lumiflavin) *in vacuo*. The atom numbering scheme is shown below.

♦Isotropic hyperfine interactions.

♣Principal anisotropic components of the hyperfine tensors (arranged in descending order of magnitude for each nucleus).

Notes:

H8 methyl group. The anisotropic components are small (< 0.08 mT) and were not included in the spin dynamics simulations. The average of the three isotropic couplings, (0.6493 + 0.6493 + 0.0212)/3 mT, was used for all three methyl protons on the assumption that methyl group rotation is fast enough to average the three interactions.

H7 methyl group. The anisotropic components are small (< 0.05 mT) and were not included in the spin dynamics simulations. The average of the three isotropic couplings, −(0.2011 + 0.2011 + 0.0225)/3 mT, was used for all three methyl protons on the assumption that methyl group rotation is fast enough to average the three interactions.

Hβ. The anisotropic components are small (< 0.09 mT) and were not included. The β protons were assigned isotropic hyperfine couplings equal to the largest of the three calculated for the N(10) methyl group in lumiflavin (0.4070, 0.4070, −0.0189 mT).

Choice of nuclei. The spin dynamics calculations reported in the main text included the following 7 nuclei: N5, N10, H6, 3×H8, 1×Hβ.

The *DFT calculations* were performed separately for the two radicals on the assumption that the 1.9 nm centre-to-centre distance between them in the protein is large enough that the hyperfine interactions should be very similar in the radical pair.

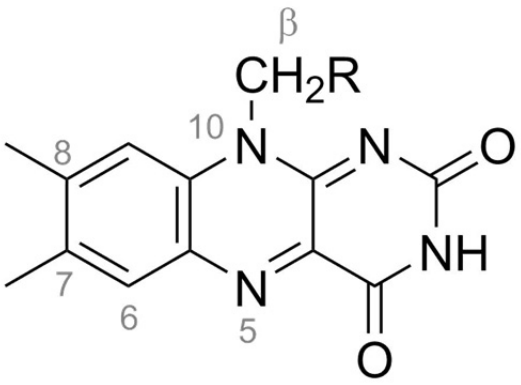

Table S2. Hyperfine tensors for the $TrpH^{\bullet+}$ radical.♥

Nucleus	**A** ♠	a_{iso}/mT♦	T_{qq}/mT ♣
N1	$\begin{pmatrix} -0.0336 & 0.0924 & -0.1354 \\ 0.0924 & 0.3303 & -0.5318 \\ -0.1354 & -0.5318 & 0.6680 \end{pmatrix}$	0.3215	0.7596 −0.3745 −0.3851
H1	$\begin{pmatrix} -0.9920 & -0.2091 & -0.2003 \\ -0.2091 & -0.2631 & 0.2803 \\ -0.2003 & 0.2803 & -0.5398 \end{pmatrix}$	−0.5983	0.5914 −0.1071 −0.4843
H2	$\begin{pmatrix} -0.2843 & 0.1757 & 0.1525 \\ 0.1757 & -0.2798 & 0.0975 \\ 0.1525 & 0.0975 & -0.2699 \end{pmatrix}$	−0.2780	0.2855 −0.0919 −0.1936
H4	$\begin{pmatrix} -0.5596 & -0.1956 & -0.1657 \\ -0.1956 & -0.4020 & 0.0762 \\ -0.1657 & 0.0762 & -0.5021 \end{pmatrix}$	−0.4880	0.3001 −0.0480 −0.2520
H6	$\begin{pmatrix} -0.0506 & 0.0622 & 0.0889 \\ 0.0622 & -0.3100 & -0.0297 \\ 0.0889 & -0.0297 & 0.2642 \end{pmatrix}$	−0.2083	0.1979 −0.0494 −0.1485
H7	$\begin{pmatrix} -0.4355 & -0.1541 & -0.1239 \\ -0.1541 & -0.2777 & 0.0864 \\ -0.1239 & 0.0864 & -0.3770 \end{pmatrix}$	−0.3636	0.2540 −0.0594 −0.1945
Hβ1	$\begin{pmatrix} 1.5808 & -0.0453 & -0.0506 \\ -0.0453 & 1.5575 & 0.0988 \\ -0.0506 & 0.0988 & 1.6752 \end{pmatrix}$	1.6046	0.1521 −0.0456 −0.1065
Hα	$\begin{pmatrix} -0.0601 & 0.0037 & 0.0331 \\ 0.0037 & -0.0251 & 0.0111 \\ 0.0331 & 0.0111 & -0.1940 \end{pmatrix}$	−0.0931	−0.1092 0.0395 0.0698
N*	$\begin{pmatrix} 0.1295 & -0.0134 & 0.0075 \\ -0.0134 & 0.1729 & -0.0249 \\ 0.0075 & -0.0249 & 0.1371 \end{pmatrix}$	0.1465	−0.0224 −0.0207 0.0431

Hβ2	$\begin{pmatrix} 0.1634 & -0.0230 & -0.0064 \\ -0.0230 & -0.0082 & 0.0158 \\ -0.0064 & 0.0158 & -0.0182 \end{pmatrix}$	0.0457	–0.0758 –0.0454 0.1211
H5	$\begin{pmatrix} 0.0051 & 0.0616 & 0.0694 \\ 0.0616 & -0.0665 & 0.0391 \\ 0.0694 & 0.0391 & -0.0586 \end{pmatrix}$	–0.0400	–0.0632 –0.0616 0.1248

♥Calculated by Dr Ilya Kuprov, Department of Chemistry, University of Southampton using density functional theory in Gaussian-03 (1) at the UB3LYP/EPR-III level (2). The calculation was done for the radical cation of tryptophan *in vacuo*. The atom numbering scheme is shown below.

♠Full hyperfine tensors in the same axis system as $FAD^{\bullet-}$ (Table S1). The relative orientation of the two radicals was taken to be that of the FAD cofactor and Trp-342 (the terminal tryptophan of the Trp-triad) in the crystal structure of *Drosophila melanogaster* cryptochrome (*Dm*Cry, PDB entry 4GU5 (3, 4)).

♦Isotropic hyperfine interactions.

♣Principal anisotropic components of the hyperfine tensors (arranged in descending order of magnitude for each nucleus).

*The nitrogen of the NH_2 group.

Notes:

Choice of nuclei. The spin dynamics calculations reported in the main text included the following 7 nuclei: N1,H1, H2, H4, H5, H7, Hβ1.

The DFT calculations were performed separately for the two radicals on the assumption that the 1.9 nm centre-to-centre distance between them in the protein is large enough that the hyperfine interactions should be very similar in the radical pair.

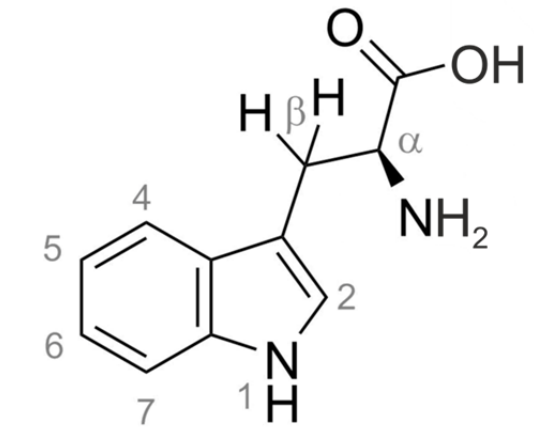

The relative orientation of the two radicals was taken to be that of FAD and Trp-342 in *Drosophila melanogaster* cryptochrome (PDB entry 4GU5, A chain) (3, 4) and is depicted below.

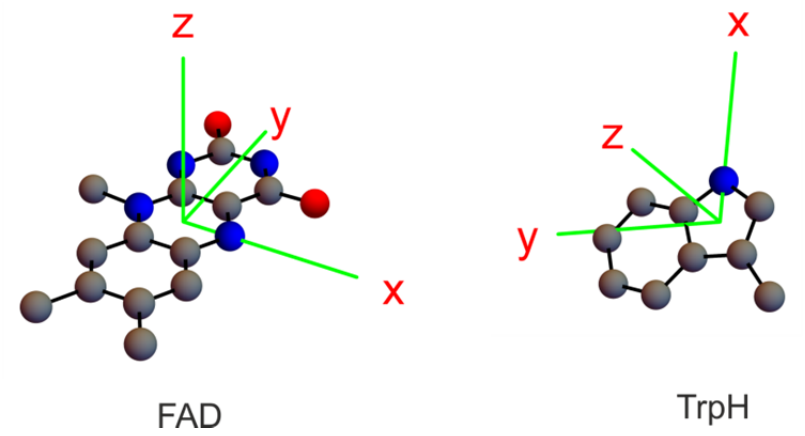

In each radical, the *z*-axis is the normal to the plane of the aromatic ring system. The angle between the two *z*-axes is 39.2°. The rotation matrix that maps the (*x*, *y*, *z*) axes of the tryptophan indole group onto those of the FAD isoalloxazine group is:

$$R = \begin{pmatrix} -0.3454 & 0.6869 & -0.6395 \\ -0.8269 & 0.0995 & 0.5535 \\ 0.4438 & 0.7199 & 0.5336 \end{pmatrix}.$$

S2. [FAD$^{\bullet-}$ TrpH$^{\bullet+}$] simulations with ≥14 nuclear spins included

Fig. S1 shows the effect on the reaction yield anisotropy of increasing the number of nuclear spins, *N*, included in the calculation (cf. *N* = 14 in Fig. 1C in the main text). The five polar plots are drawn on the same scale. The *N*/2 nuclear spins in each radical were taken in order (left to right) from Table S3. The hyperfine tensors are given in Section S1.

Although the spike is somewhat attenuated by the extra nuclei, it is relatively much less affected than the broad background signal.

Table S3. Nuclei included in the calculations.

FAD$^{\bullet-}$	N5	N10	H6	H8	H8	H8	Hβ	Hβ	H7	H7	H7
TrpH$^{\bullet+}$	N1	H1	H2	H4	H6	H7	Hβ1	Hα	N*	Hβ2	H5

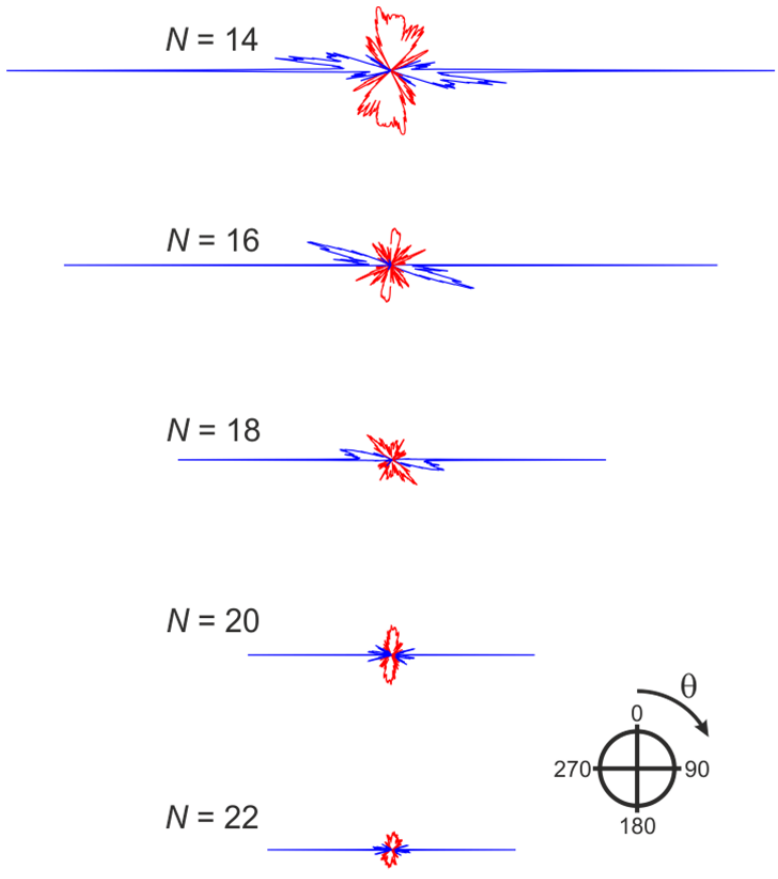

Fig. S1. Two-dimensional polar plots of the anisotropic part of Φ_S (as in Fig. 1C). Red and blue indicate values respectively larger and smaller than the isotropic value.

S3. Asymmetric recombination kinetics

The calculations presented in the main text were all performed for a reaction scheme in which singlet and triplet radical pairs recombined spin-selectively with identical rate constants ($k_S = k_T = k = \tau^{-1}$) to form distinct products. Calculations, shown in Fig. S2, performed for the toy radical pair [$X^\bullet$ $Y^\bullet$] (with one ^{14}N hyperfine interaction in each radical – as in Fig. 2C) show that the spike at $\theta = 90°$ persists even when the two rate constants differ by an order of magnitude.

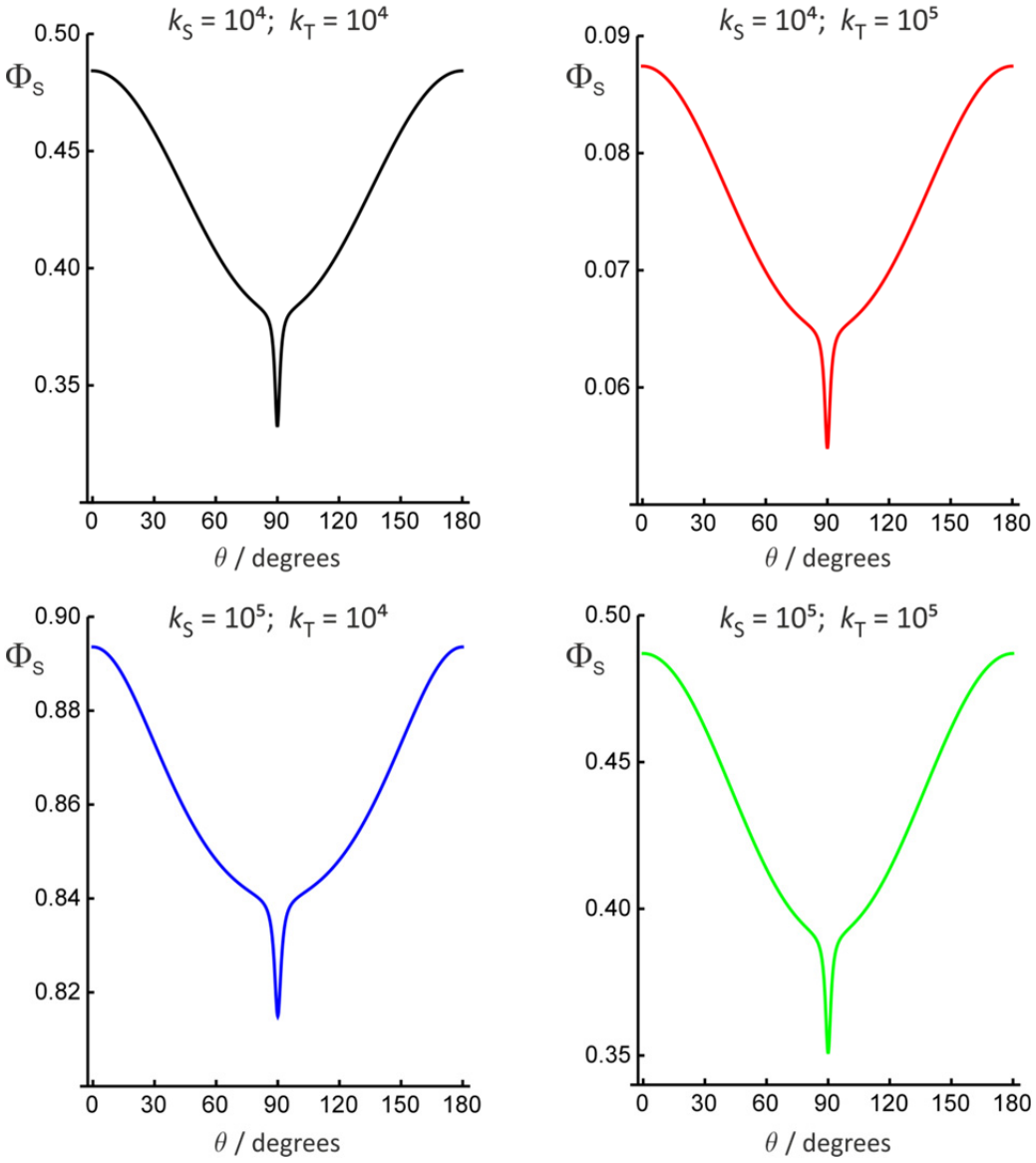

Fig. S2. Φ_S for a toy radical pair, [$X^\bullet$ $Y^\bullet$]. $X^\bullet$ contains a single ^{14}N hyperfine tensor with principal components (A_{xx}, A_{yy}, A_{zz}) = (–0.0989, –0.0989, 1.7569) mT (based on N5 in $FAD^{\bullet-}$). $Y^\bullet$ contains a single ^{14}N nucleus with (A_{xx}, A_{yy}, A_{zz}) = (0.0, 0.0, 1.0812) mT (based on N1 in $TrpH^{\bullet+}$). The two hyperfine tensors have parallel *z*-axes. The singlet and triplet recombination rate constants (s^{-1}) are as indicated.

S4. Exchange and dipolar interactions

Preliminary simulations using the toy radical pair model suggest that the spike can be affected by the exchange and dipolar interactions of the electron spins in the two radicals. These effects are probably less pronounced for radicals with many nuclear spins but this is difficult to verify because the Liouville-space calculations required when electron-electron interactions are included become prohibitively slow for realistic spin systems. The effects of spin-spin interactions may also be reduced by the partial cancellation of the exchange and dipolar contributions predicted for a radical pair with a separation close to that of $FAD^{\bullet-}$ and $TrpH^{\bullet+}$ in cryptochrome (5). Finally, if in a migratory bird cryptochrome, as in *Xenopus laevis* (6-4) photolyase (6), there are four instead of three Trp residues involved in photoreduction of the FAD, then the magnetically sensitive FAD-Trp radical pair could have a larger distance between the radical centres and consequently smaller spin-spin interactions.

S5. Calculation of Φ_S in the absence of molecular motion

Magnetic field effects were modelled by means of the following reaction scheme.

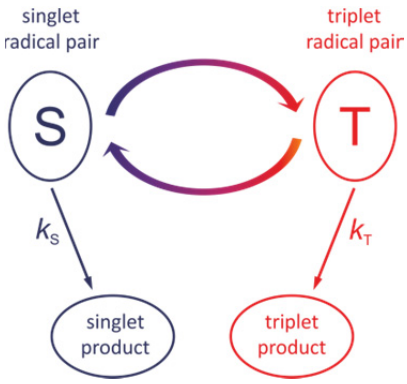

'Singlet' (S) and 'triplet' (T) refer to the states of the two electron spins, one in each radical. The curved arrows represent the coherent spin dynamics arising from the combined effects of Zeeman and hyperfine interactions. The straight arrows are spin-selective reaction steps. The radical pair is created in a singlet state by spin-conserving electron transfer. Singlet and triplet radical pairs are considered to undergo separate spin-conserving reverse electron transfer reactions to form distinct singlet and triplet products. Abstract examples of such reactions are $^{S}\left[A^{\bullet+}B^{\bullet-}\right] \rightarrow {}^{S}A + {}^{S}B$ and $^{T}\left[A^{\bullet+}B^{\bullet-}\right] \rightarrow {}^{T}A + {}^{S}B$ where ^{S}A and ^{S}B are diamagnetic (closed shell, singlet state) molecules with no unpaired electron spins and ^{T}A is a paramagnetic molecular triplet. In the model, the rate constants of these two reactions are identical: $k_S = k_T = k = 1/\tau$. We calculate Φ_S, the fractional yield of the singlet product once all radical pairs have reacted. Φ_S is related to the yield of the triplet product by $\Phi_T = 1 - \Phi_S$.

The singlet yield Φ_S was calculated as (7, 8):

$$\Phi_S = k\int_0^\infty p_S(t)\,\mathrm{e}^{-kt}\,\mathrm{d}t$$

in which $k = k_S = k_T$ is the recombination rate constant and $p_S(t)$ is the fraction of radical pairs in the singlet state at time t (9):

$$p_S(t) = \frac{1}{4} + \sum_{p=x,y,z}\sum_{q=x,y,z} R_{pq}^{(\mathrm{A})}(t)R_{pq}^{(\mathrm{B})}(t)$$

with

$$R_{pq}^{(m)}(t) = \frac{1}{Z_m}\mathrm{Tr}\left[\hat{S}_{mp}\mathrm{e}^{-\mathrm{i}\hat{H}_m t}\hat{S}_{mq}\mathrm{e}^{\mathrm{i}\hat{H}_m t}\right]$$

and

$$Z_m = \prod_{j=1}^{N_m}\left(2I_{mj}+1\right).$$

$\hat{S}_{mp}$ ($p = x,y,z$) are the electron spin operators and $\hat{H}_m$ is the spin Hamiltonian of radical m (m = A, B). I_{mj} is the spin quantum number of nucleus j in radical m and N_m is the number of nuclei in radical m.

The spin Hamiltonian for each radical contains terms for the Zeeman interaction (Z) of the electron spin with the applied magnetic field, and the various hyperfine interactions (HFI) in the two radicals:

$$\hat{H}_m = \hat{H}_{m,\mathrm{Z}}(\theta,\phi) + \hat{H}_{m,\mathrm{HFI}}$$

with

$$\hat{H}_{m,\mathrm{Z}}(\theta,\phi) = \gamma_{\mathrm{e}} B_0 \left[\hat{S}_{mx} \sin\theta\cos\phi + \hat{S}_{my} \sin\theta\sin\phi + \hat{S}_{mz} \cos\theta \right]$$

and

$$\hat{H}_{m,\mathrm{HFI}} = \sum_{j=1}^{N_m} \left[a_{mj}^{\mathrm{iso}} \hat{\mathbf{S}}_m \bullet \hat{\mathbf{I}}_{mj} + \hat{\mathbf{S}}_m \bullet \mathbf{T}_{mj} \bullet \hat{\mathbf{I}}_{mj} \right]$$

where B_0 is the strength of the external magnetic field, θ and ϕ define its direction with respect to the radical pair, a_{mj}^{iso} is the isotropic hyperfine coupling constant and $\mathbf{T}_{mj}$ is the anisotropic part of the hyperfine interaction tensor of nucleus j coupled to electron m. $\hat{\mathbf{I}}_{mj}$ is the nuclear spin operator of nucleus j coupled to electron m.

The main text summarizes the conditions under which the simulations were performed.

S6. Visual modulation patterns

"Visual modulation patterns", first calculated by Ritz *et al*. (10), are crude representations of a bird's perception of the compass information delivered by an array of cryptochrome-containing magnetoreceptor cells distributed around its retina. The proteins are assumed to be identically oriented in every cell and each cell to be identically oriented with respect to the local retina normal. Cells at different locations in the retina have different orientations with respect to the geomagnetic field and therefore deliver different directional information. The assumption is that either by comparing the signals from different parts of the retina or by performing head scans, or both, the bird would obtain information sufficient to orient itself. As noted by Ritz *et al*. (11), different arrangements of the cryptochromes, e.g. a perpendicular orientation of the proteins in neighbouring cells, can result in different sensitivity to the geomagnetic field. However, the clarity of the sensory information for these alternative arrangements would be similar to that of the simulations used here for illustrative purposes.

The visual modulation patterns for [$FAD^{\bullet-}$ $TrpH^{\bullet+}$] in Fig. 1E were calculated as described by Lau *et al*. (12). The cells were assumed to have no preferred orientation with respect to rotation around the local retina normal (13). This ordering is not unlike that of the rod and cone visual receptor cells in the retina (one of the proposed locations for cryptochrome magnetoreceptors (13, 14)). The signals were therefore integrated over the angle η (defined in the Electronic Supplementary Material of Ref. (12)). The *z*-axes of the FAD molecules within each cell were assumed to be perpendicular to this symmetry axis so that the η-averaging of Φ_S is around an axis in the *xy*-plane of the flavin ring system. Fig 1F was calculated from Fig. 1D using the same averaging.

Fig. S3 summarizes the geometry of the model and the various rotations. In the visual modulation patterns, θ varies from zero at the centre of the pattern to 90° at the edge. ϕ increases anticlockwise from zero at the bottom.

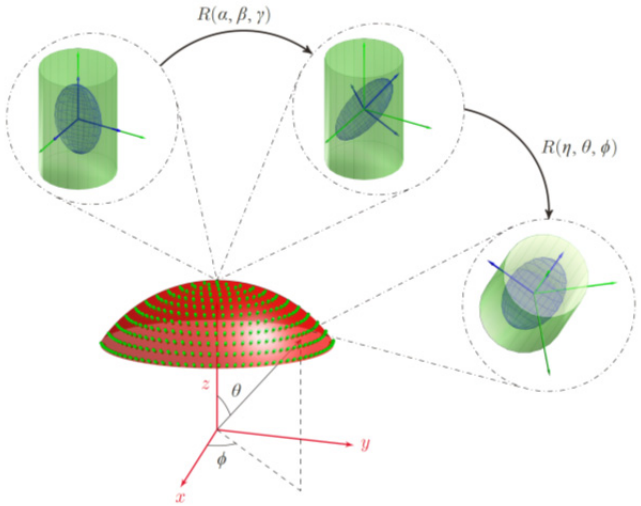

Fig. S3. Cells (green spots) are distributed around the retina (red dome). Euler angles (α,β,γ) define the orientation of cryptochrome molecules (blue) within each cell. Euler angles (η,θ,ϕ) define the position of the cell in the retina. η specifies the rotation of the cell around its *z*-axis, shown here as a cylindrical symmetry axis. Taken from Ref. (15).

S7. Hyperfine interactions of flavin radicals in proteins

Table S4 summarizes the available experimental measurements of the hyperfine tensor components of the N5 and N10 nitrogens in flavin radicals in proteins. Also included at the bottom of the Table are some DFT calculations of hyperfine interactions in a neutral flavin radical for comparison with those used in the present study. Additionally, Eriksson & Ehrenberg (16) reported $A_{xx} = A_{yy} = 0.25a_{\text{iso}}$ and $A_{zz} = 2.5a_{\text{iso}}$ for a flavin radical in *Azotobacter vinelandii* NADPH dehydrogenase.

All values are given in MHz. The principal components, A_{qq}, are related to the quantities in Table S1 by $A_{qq} = a_{\text{iso}} + T_{qq}$.

Although the values of A_{xx}, A_{yy}, and A_{zz} vary considerably, in all cases $A_{zz} > 10|A_{xx}|, 10|A_{yy}| \neq 0$, as required for the existence of a spike in Φ_S.

Table S4. Hyperfine tensor components of flavin radicals

protonation state of flavin	protein	reference		$A_{xx} = A_{yy}$ ♣	A_{zz} ♣
neutral	*Anabaena* flavodoxin	(17)	N10	3 ± 1	31 ± 1
neutral	*Anabaena* ferredoxin $NADP^+$ reductase	(18)	N10	2.7 ± 1.3	29.7 ± 1.9
neutral	Na^+ translocating NADH:quinone oxidoreductase *Vibrio cholerae*	(19)	N5	0.2 ± 2.0	52.5 ± 0.5
			N10	2.0 ± 1.0	28.9 ± 0.6
anionic	Na^+ translocating NADH:quinone oxidoreductase *Vibrio cholerae*	(19)	N5	2.3 ± 0.6	57.6 ± 0.5
			N10	1.6 ± 0.6	22.8 ± 0.6

protonation state of flavin	calculation	reference		$A_{xx} = A_{yy}$	A_{zz}
anionic	DFT UB3LYP/EPR-III	This work	N5	−2.6	49.2
			N10	−0.5	16.9
neutral ♥	DFT B3LYP/EPR-II	(20)	N5	−0.5	40.6
			N10	−0.8	19.3
neutral ♠	DFT B3LYP/EPR-II	(20)	N5	−1.7	42.7
			N10	0.9	23.1

♣The signs of the A_{qq} values were not determined.
♥$FADH^\bullet$ with the ribityl side chain truncated after the C3′ carbon.
♠$FADH^\bullet$ with the ribityl side chain truncated after the C3′ carbon, with amino acid fragments included to mimic the protein environment of FAD in *E. coli* DNA photolyase.

S8. Avoided energy-level crossings

We demonstrate here that the spike can be unambiguously attributed to avoided crossings of the quantum mechanical energy levels of the radical pair spin Hamiltonian as a function of the magnetic field direction.

In the case that singlet and triplet react to form separate products with the same rate constant k, Φ_S may be obtained from (7):

$$\Phi_S = \frac{1}{Z}\sum_m\sum_n \left|P^S_{mn}\right|^2 \frac{k^2}{k^2+\left(\omega_m-\omega_n\right)^2} \ . \tag{1}$$

Z is the total number of nuclear spin configurations and $\hat{P}^S$ is the singlet projection operator with matrix elements $P^S_{mn} = \langle m|\hat{P}^S|n\rangle$. $|n\rangle$ and $|m\rangle$ are eigenstates of the radical pair spin Hamiltonian, $\hat{H} = \hat{H}_A + \hat{H}_B$, with eigenvalues ω_n and ω_m respectively.

We consider two basis states, $|1\rangle$ and $|2\rangle$, with the following Hamiltonian matrix elements ($H_{jk} = \langle j|\hat{H}|k\rangle$):

$$H_{11} = +aq; \ \ H_{22} = -aq; \ \ H_{12} = H_{21} = b\,, \tag{2}$$

where the variable q defines the direction of the magnetic field relative to the radical pair. q corresponds to the angle $\theta - 90°$ in the main text. a plays the role of A_{zz} and the weak Zeeman interaction; b plays the role of $\sqrt{A_{xx}^2 + A_{yy}^2}$. The latter can be regarded as a small perturbation. The A_{zz} term together with the interaction of the electron spins with the external magnetic field causes the energy levels to vary approximately linearly in the neighbourhood of θ = 90° (hence the $\pm aq$ terms). A_{xx} and A_{yy} (the b term) couple the two states and lead to the avoided crossing when $\theta \approx 90°$.

Solving the secular equations for this two-level system gives the eigenvalues $\varepsilon_\pm$ and eigenvectors $|\pm\rangle$:

$$\varepsilon_\pm = \pm\sqrt{a^2q^2+b^2} \tag{3}$$

$$\begin{aligned} |+\rangle &= \cos\zeta|1\rangle + \sin\zeta|2\rangle \\ |-\rangle &= \sin\zeta|1\rangle - \cos\zeta|2\rangle \end{aligned}, \tag{4}$$

where

$$\tan 2\zeta = \frac{b}{aq}\,. \tag{5}$$

When $b = 0$, the energy levels cross at q = 0 ($\varepsilon_\pm = 0$); when $b \neq 0$, this becomes an avoided crossing ($\varepsilon_\pm = \pm b$). Assuming

$$P^S_{11} = p_1, \quad P^S_{22} = p_2, \quad P^S_{12} = P^S_{21} = 0 \tag{6}$$

i.e. that the basis states have different singlet characters (p_1 and p_2), one finds:

$$\begin{aligned} P^S_{++} &= \Sigma + \Delta\cos(2\zeta) \\ P^S_{--} &= \Sigma - \Delta\cos(2\zeta) \\ P^S_{+-} &= P^S_{-+} = \Delta\sin(2\zeta) \end{aligned} \tag{7}$$

where $\Sigma = \frac{1}{2}(p_1 + p_2)$ and $\Delta = \frac{1}{2}(p_1 - p_2)$. Using eqn (1) and omitting *Z*, the contribution of these two levels to the singlet yield is:

$$\Phi_S^{\pm} = \left(P_{++}^S\right)^2 + \left(P_{--}^S\right)^2 + 2\left(P_{+-}^S\right)^2 \frac{k^2}{k^2 + 4\left(a^2q^2 + b^2\right)}. \tag{8}$$

Combining eqn (8) with eqn (7) and subtracting the singlet yield in the absence of an avoided crossing, we obtain:

$$\Phi_S^{\pm} - \Phi_S^{\pm}(b=0) = \frac{-8b^2\Delta^2}{k^2 + 4b^2 + 4a^2q^2}. \tag{9}$$

This is a negative Lorentzian function of *q*, centred at the position of the avoided crossing ($q = 0$) with amplitude

$$\frac{-8b^2\Delta^2}{k^2 + 4b^2} \tag{10}$$

and full width at half maximum height

$$\sqrt{\frac{4b^2 + k^2}{a^2}}. \tag{11}$$

It is clear from eqns (10) and (11), that as the lifetime of the radical pair is prolonged (by reducing *k*), the spike becomes stronger and narrower with the height and width tending to $-2\Delta^2$ and $2b/a$, respectively, in the limit *k* << 2*b*. In the opposite limit, *k* >> 2*b*, the spike vanishes. The other conditions for the existence of a spike in this simple model are that there is an avoided crossing ($b \neq 0$) and that the basis states have different singlet characters ($\Delta \neq 0$).

The condition, derived above, that the two energy levels involved in the avoided crossing must have different singlet characters may be used to deduce a condition on the counter-radical. Writing the pair of interacting states as

$$|\psi_1\rangle = |\phi_A\rangle|\phi_B\rangle \quad \text{and} \quad |\psi_2\rangle = |\phi'_A\rangle|\phi_B\rangle, \tag{11}$$

where A and B label the two radicals, we have:

$$\langle\psi_1|\hat{P}^S|\psi_1\rangle - \langle\psi_2|\hat{P}^S|\psi_2\rangle = \sum_{q=x,y,z}\left[\langle\phi_A|\hat{S}_{Aq}|\phi_A\rangle - \langle\phi'_A|\hat{S}_{Aq}|\phi'_A\rangle\right]\langle\phi_B|\hat{S}_{Bq}|\phi_B\rangle. \tag{11}$$

With a simple "crossing" Hamiltonian for radical A containing a single spin-$\frac{1}{2}$ nucleus (axial hyperfine interaction, $A_{xx} = A_{yy} = 0$, and the magnetic field perpendicular to the hyperfine axis):

$$\hat{H}_A = \gamma_e B_0 \hat{S}_{Ax} + A_{zz}\hat{S}_{Az}\hat{I}_z \tag{11}$$

it can be shown that

$$\langle\psi_1|\hat{P}^S|\psi_1\rangle - \langle\psi_2|\hat{P}^S|\psi_2\rangle \propto \langle\phi_B|\hat{S}_{Bz}|\phi_B\rangle \tag{11}$$

That is, for an avoided crossing to give a spike in Φ_S, we require the *z*-component of the electron spin in the counter-radical to be non-zero.

S9. Simplified FAD-containing radical pairs

Fig. S4 shows the simulations for [$FAD^{\bullet-}$ $Y^{\bullet}$] referred to in the sub-section *Simpler flavin-containing radical pairs* in the main text. A spike is not seen unless the hyperfine tensor of the single (^{14}N) nucleus in $Y^{\bullet}$ is anisotropic. The spikes at θ = 90° arise from $FAD^{\bullet-}$ (as discussed in the text). The additional spikes at θ = 45° come from $Y^{\bullet}$.

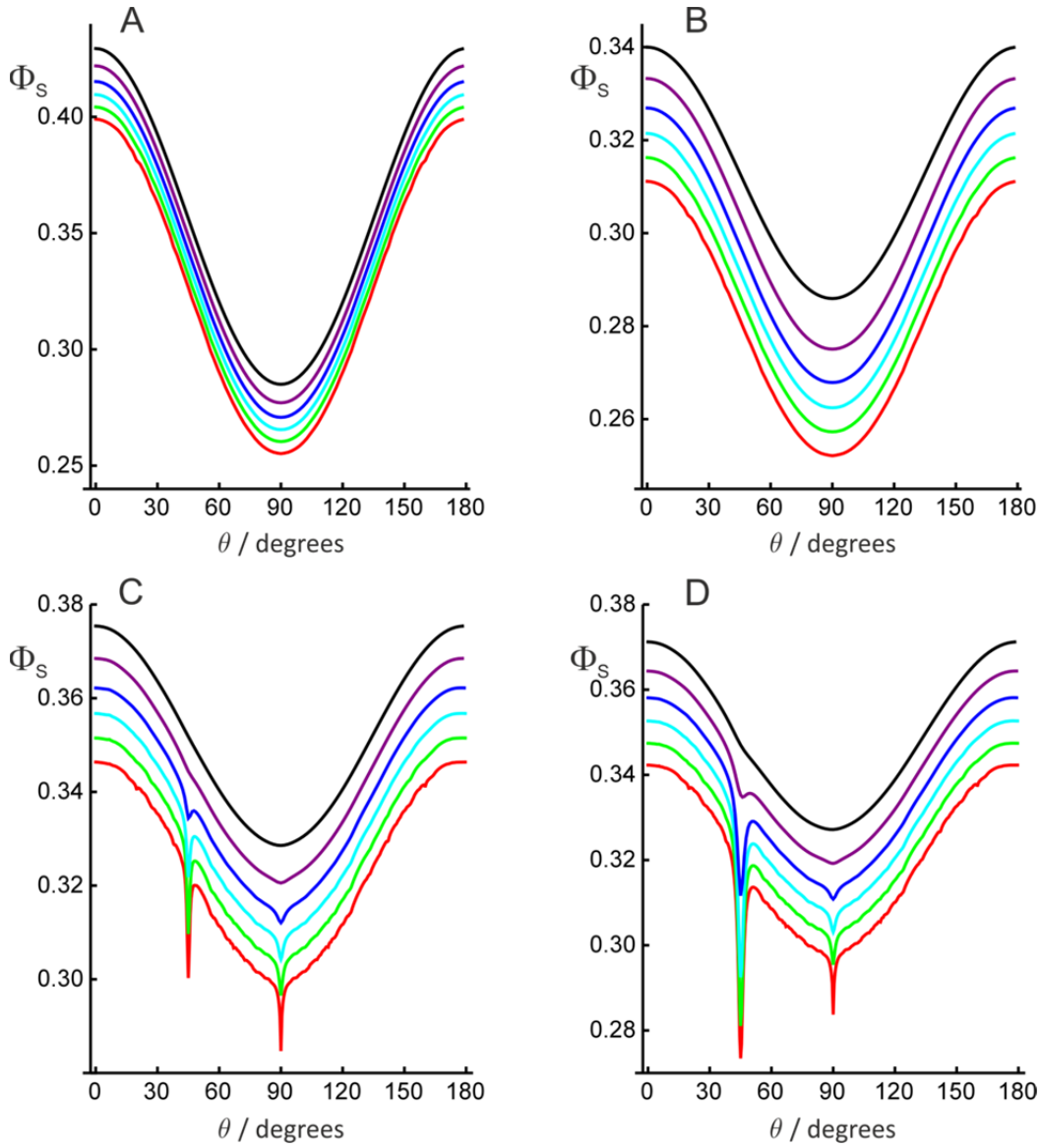

Fig. S4. Φ_S for a [$FAD^{\bullet-}$ $Y^{\bullet}$] radical pair in which radical $Y^{\bullet}$ contains a single ^{14}N nucleus. The radical pair lifetimes are as in Fig. 2B: black 1 μs, purple 2 μs, blue 5 μs, cyan 10 μs, green 20 μs, red 100 μs. The angle between the *z*-axes of $Y^{\bullet}$ and $FAD^{\bullet-}$ was 45°. For clarity, the five traces for τ < 100 μs have been offset vertically, from top to bottom, by 0.020, 0.016, 0.012, 0.008, and 0.004 respectively. The hyperfine tensors of the ^{14}N nucleus in $Y^{\bullet}$ were:

A. (A_{xx}, A_{yy}, A_{zz}) = (0.0, 0.0, 0.0)
B. (A_{xx}, A_{yy}, A_{zz}) = (0.3604, 0.3604, 0.3604) mT (isotropic)
C. (A_{xx}, A_{yy}, A_{zz}) = (–0.1, –0.1, 1.2812) mT (axial)
D. (A_{xx}, A_{yy}, A_{zz}) = (–0.2, 0.0, 1.2812) mT (rhombic)

S10. Calculation of Φ_S for radicals undergoing rotational jumps

The simulations in Fig. 3 in the main text were carried out as follows. The density operator $\rho(t)$ of a radical pair in a singlet state at time t was obtained from the Liouville equation:

$$\frac{\mathrm{d}\hat{\rho}}{\mathrm{d}t} = -\hat{\hat{L}}\hat{\rho} \;\Rightarrow\; \hat{\rho}(t) = \mathrm{e}^{-\hat{\hat{L}}t}\hat{\rho}(0) = \frac{1}{Z}\mathrm{e}^{-\hat{\hat{L}}t}\hat{P}^{\mathrm{S}}$$

in which $\hat{P}^{\mathrm{S}}$ is the singlet projection operator, Z is the number of nuclear spin configurations and the $\hat{\hat{L}}$ is the Liouvillian superoperator . The fraction of radical pairs in the singlet state, $p_{\mathrm{S}}(t)$, is:

$$p_{\mathrm{S}}(t) = \mathrm{Tr}\left[\hat{P}^{\mathrm{S}}\hat{\rho}(t)\right] = \frac{1}{Z}\mathrm{Tr}\left[\hat{P}^{\mathrm{S}}\mathrm{e}^{-\hat{\hat{L}}t}\hat{P}^{\mathrm{S}}\right]$$

and the yield of the reaction product formed from the singlet state is:

$$\Phi_{\mathrm{S}} = k\int_0^{\infty} p_{\mathrm{S}}(t)\mathrm{d}t = \frac{k}{Z}\mathrm{Tr}\left[\hat{P}^{\mathrm{S}}\hat{\hat{L}}^{-1}\hat{P}^{\mathrm{S}}\right]$$

in which k is the recombination rate constant for singlet and triplet states ($k = \tau^{-1}$). L and ρ, the matrix representations of $\hat{\hat{L}}$ and $\hat{\rho}$ respectively, were constructed from the matrix representations of the Liouvillians and density operators for the two sites, $L_{\pm}$ and $\rho_{\pm}$:

$$L = \begin{pmatrix} L_{+} + k_{\mathrm{r}}E & -k_{\mathrm{r}}E \\ -k_{\mathrm{r}}E & L_{-} + k_{\mathrm{r}}E \end{pmatrix} \quad \text{and} \quad \rho = \begin{pmatrix} \rho_{+} \\ \rho_{-} \end{pmatrix}$$

where k_{r} is the rocking rate constant. E is the identity matrix. $L_{\pm}$ have dimension $4Z^2$. $\rho_{\pm}$ are column vectors with the same dimension. $L_{\pm}$ were obtained from the corresponding spin Hamiltonians:

$$L_{\pm} = \mathrm{i}\left[H_{\pm}\otimes E - E\otimes H_{\pm}^{\mathrm{T}}\right] + kE$$

with (see Section S5):

$$\hat{H}_{\pm} = \gamma_{\mathrm{e}}B_0\left[\left(\hat{S}_{\mathrm{A}x}+\hat{S}_{\mathrm{B}x}\right)\sin\theta\cos\phi + \left(\hat{S}_{\mathrm{A}y}+\hat{S}_{\mathrm{B}y}\right)\sin\theta\sin\phi + \left(\hat{S}_{\mathrm{A}z}+\hat{S}_{\mathrm{B}z}\right)\cos\theta\right]$$
$$+\sum_{n=1}^{N_{\mathrm{A}}} a_{\mathrm{A}n}^{\mathrm{iso}}\hat{\mathbf{S}}_{\mathrm{A}}.\hat{\mathbf{I}}_{\mathrm{A}n} + \sum_{m=1}^{N_{\mathrm{B}}} a_{\mathrm{B}m}^{\mathrm{iso}}\hat{\mathbf{S}}_{\mathrm{B}}.\hat{\mathbf{I}}_{\mathrm{B}m} + \sum_{n=1}^{N_{\mathrm{A}}}\hat{\mathbf{S}}_{\mathrm{A}}.\mathbf{R}_{\pm}^{-1}.\mathbf{T}_{\mathrm{A}n}.\mathbf{R}_{\pm}.\hat{\mathbf{I}}_{\mathrm{A}n} + \sum_{m=1}^{N_{\mathrm{B}}}\hat{\mathbf{S}}_{\mathrm{B}}.\mathbf{T}_{\mathrm{B}m}.\hat{\mathbf{I}}_{\mathrm{B}m}$$

The matrices that rotate radical A between the two sites are given by:

$$\mathbf{R}_{\pm} = \cos\beta\mathbf{E} \pm \sin\beta\begin{pmatrix} 0 & -u_z & u_y \\ u_z & 0 & -u_x \\ -u_y & u_x & 0 \end{pmatrix} + (1-\cos\beta)\begin{pmatrix} u_x^2 & u_xu_y & u_xu_z \\ u_xu_y & u_y^2 & u_yu_z \\ u_xu_z & u_yu_z & u_z^2 \end{pmatrix}$$

where the unit vector (u_x, u_y, u_z) is the rotation axis and β is the rotation angle.

S11. Amplitudes and widths of the spike for radicals undergoing rotational jumps

To obtain a more quantitative picture of the way in which the spike is affected by two-site hopping, the singlet yields in Fig. 3A for the toy radical pair were fitted to a function of the form:

$$a + b\cos^2\theta - \frac{Hw^2}{(\theta-\theta_0)^2 + w^2} .$$

That is, the rolling background was approximately modelled as $a + b\cos^2\theta$ and the spike by an inverted Lorentzian of amplitude H, width $2w$, centred at $\theta = \theta_0$. The dependence of H (left) and w (right) on the hopping rate constant are shown in Fig. S5, together with the values for the static case with no hopping (extreme right hand side of each plot). While the amplitude drops as the hopping becomes slower, there is hardly any change in the width.

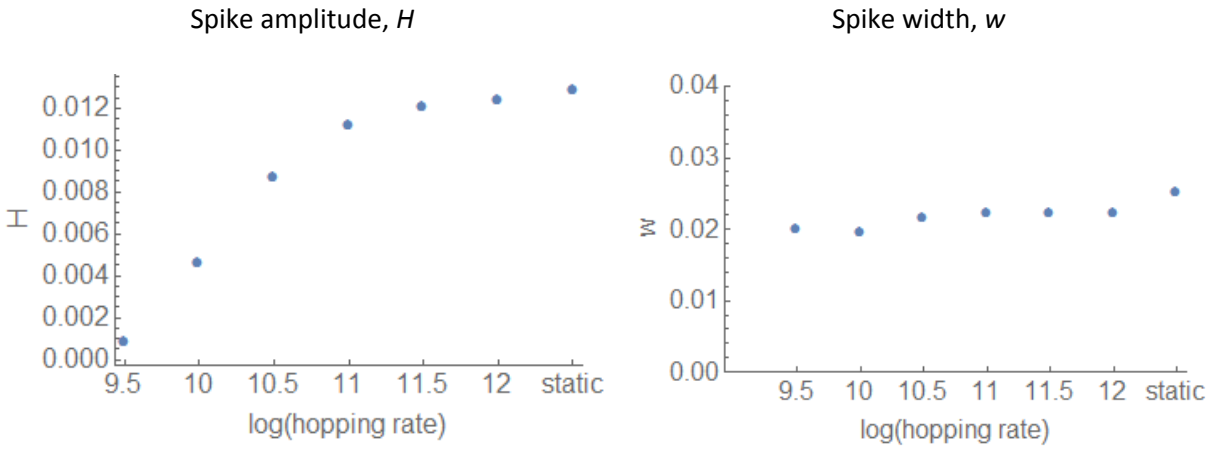

Fig. S5. Variation of the amplitude and width of the spike in Fig. 3A with rate constant k_r.

S12. Φ_S for [X$^\bullet$ Y$^\bullet$] radical pair undergoing slow rotational jumps

Fig. S6 compares Fig. 3A from the main text (3×10^{11} s$^{-1} \geq k_r \geq 1 \times 10^8$ s^{-1} (reproduced here as Fig. S6A) with the corresponding simulations for 1×10^8 s$^{-1} \geq k_r \geq 1 \times 10^5$ s^{-1} (Fig. S6B). Sharp spikes are seen when the rocking is either fast ($k_r \geq 3 \times 10^9$ s^{-1}) or slow ($k_r \leq 3 \times 10^6$ s^{-1}).

In the intermediate regime (10^7 s$^{-1} \leq k_r \leq 10^9$ s^{-1}), where k_r is comparable to the strengths of the hyperfine interactions, spin relaxation is fast and results in attenuation of both the spike and the broad background. The loss of spin-correlation is most efficient when $k_r \approx 1 \times 10^8$ s^{-1}, with Φ_S tending towards 0.25, the statistical singlet fraction expected for an equilibrated radical pair.

As the value of k_r is reduced from 1×10^8 s^{-1} (Fig. S6B), the spike at $\theta = 90°$ reappears when $k_r = 3 \times 10^6$ s^{-1} and splits into two (at $\theta = 90 \pm 5°$) when $k_r \leq 3 \times 10^5$ s^{-1}, corresponding to static disorder on the timescale of the radical pair lifetime, τ.

In principle, the pair of sharp spikes seen for the slowest rocking rates in Fig. S6B ($k_r \leq 3 \times 10^5$ s^{-1}) could afford directional information. However it is not likely that a radical would, in reality, jump between just two well-defined orientations. More realistically, there would be a distribution of thermally accessible orientations so that, in the slow motion limit, the spike would be broadened to an extent that reflected the static distribution of internal magnetic interactions. A sharp spike and precise directional information are therefore much more likely to be found in the fast motion regime ($k_r \geq 3 \times 10^9$ s^{-1} in Fig. S6A).

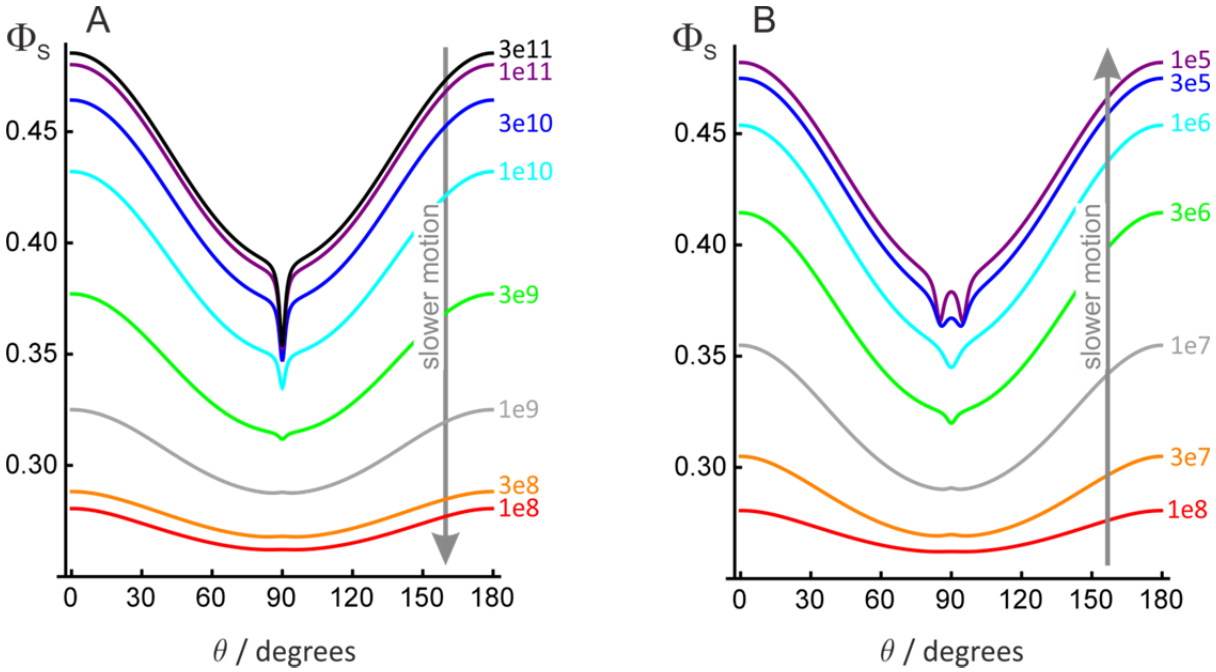

Fig. S6. Φ_S for the toy radical pair, [X$^\bullet$ Y$^\bullet$]. X$^\bullet$ has a single ^{14}N nucleus with hyperfine components (A_{xx}, A_{yy}, A_{zz}) = (–0.2, –0.2, 1.7569) mT; Y$^\bullet$ has a single ^{14}N nucleus with hyperfine components (0.0, 0.0, 1.0812) mT. The two hyperfine tensors have parallel *z*-axes. The radical pair lifetime is 10 μs. X$^\bullet$ underwent 10° jumps (i.e. β = 5°) around the *y*-axis with rate constants k_r (A) between 3×10^{11} s^{-1} and 1×10^8 s^{-1} and (B) between 1×10^8 s^{-1} and 1×10^5 s^{-1}, as indicated.

We have modelled the spin relaxation that arises from modulation of the hyperfine interactions by librational motions of the radicals within the protein. An additional source of relaxation is the time-dependence of the electron-electron exchange and dipolar interactions arising from fluctuations in the radical-radical separation. Interestingly, this relaxation mechanism can boost the anisotropy of Φ_S by relaxing the spins more efficiently for some directions of the magnetic field than for others. This will be the subject of a future publication.

S13. Φ_S for [X$^{\bullet}$ TrpH$^{\bullet+}$] radical pair in which TrpH$^{\bullet+}$ undergoes rotational jumps

Fig. 3B from the main text (reproduced here as Fig. S7A) shows simulations for a [FAD$^{\bullet-}$ Y$^{\bullet}$] radical pair including the spin relaxation that results from the FAD$^{\bullet-}$ radical undergoing 10° rotational jumps (i.e. $\beta = 5°$). Fig. S7B shows the corresponding simulations for a [X$^{\bullet}$ TrpH$^{\bullet+}$] radical pair in which the TrpH$^{\bullet+}$ radical undergoes the same rotational jumps.

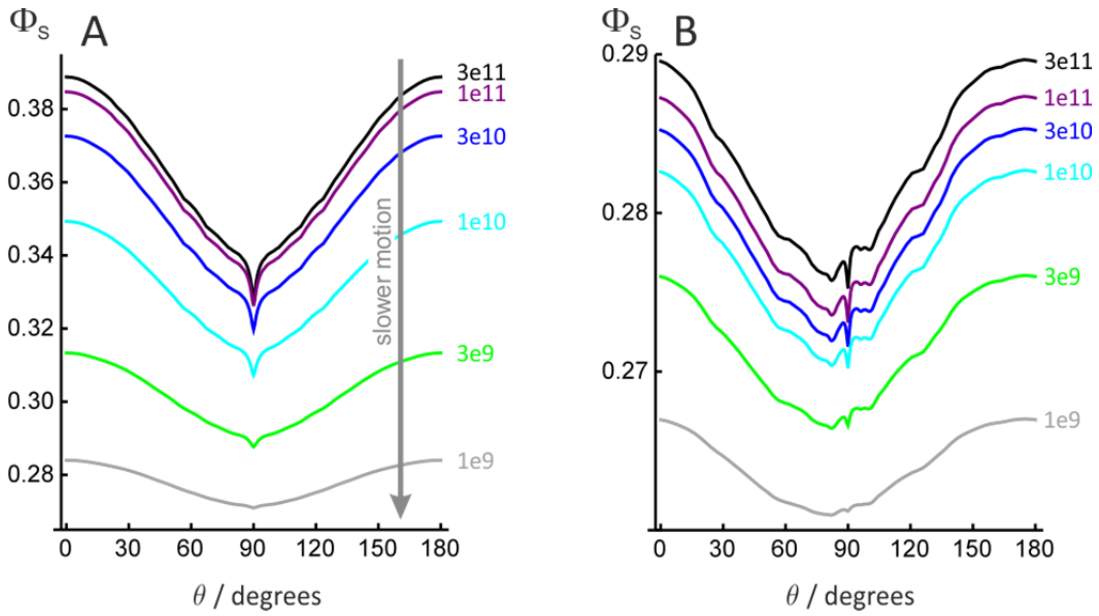

Fig. S7. Φ_S for (A) a [FAD$^{\bullet-}$ Y$^{\bullet}$] and (B) a [X$^{\bullet}$ TrpH$^{\bullet+}$] radical pair with the FAD$^{\bullet-}$ and TrpH$^{\bullet+}$ radicals undergoing 10° rotational jumps (i.e. $\beta = 5°$). Y$^{\bullet}$ has a single ^{14}N nucleus with hyperfine components (A_{xx}, A_{yy}, A_{zz}) = (0.0, 0.0, 1.0812) mT. X$^{\bullet}$ has a single ^{14}N nucleus with hyperfine components (A_{xx}, A_{yy}, A_{zz}) = (–0.1002, –0.0868, 1.7569) mT. In both cases, the radical pair lifetime was 10 μs. The rate constants (k_r) for the rocking motion are: black 3×10^{11} s^{-1}, purple 1×10^{11} s^{-1}, blue 3×10^{10} s^{-1}, cyan 1×10^{10} s^{-1}, green 3×10^{9} s^{-1}, grey 1×10^{9} s^{-1}.

S14. Precision of compass bearing

A rough idea of the precision of the compass bearing available from any given $\Phi_S(\theta)$ ($0 \leq \theta \leq 180°$) may be obtained as follows by considering the effect of stochastic detector noise. $\Phi_S(\theta)$ was calculated for a range of values of θ; random numbers, drawn from a Gaussian distribution with mean 0.0 and standard deviation σ, were added to give a noisy 'signal', $\tilde{\Phi}_S(\theta)$. The compass bearing available from $\tilde{\Phi}_S(\theta)$ was taken to be $\tilde{\theta}$, the value of θ corresponding to the minimum value of $\tilde{\Phi}_S(\theta)$. If the signal-to-noise ratio is not too low, $\tilde{\theta}$ should be close to 90° for the (noise-free) signals in Fig. 1B. The calculation was repeated 10^4 times with the same $\Phi_S(\theta)$ and a fresh set of random noise each time, drawn from the same Gaussian distribution. The uncertainty in the compass bearing, Ξ, is defined as the standard deviation of the 10^4 values of $\tilde{\theta}$. One can expect that a sharper and stronger spike will deliver a more precise compass bearing and consequently a smaller value of Ξ. Similarly, the lower the noise level, σ, the smaller Ξ should be.

To compare the performance of [$FAD^{\bullet-}$ $TrpH^{\bullet+}$] for different lifetimes under the conditions of Fig. 1, we determined, for each value of τ, the amount of noise (σ) that could be introduced before Ξ exceeded 1°. The results are shown in Table S5.

Table S5. Values of the noise level σ that would allow direction sensing with a precision of 1° using the signals shown in Fig. 1 for [$FAD^{\bullet-}$ $TrpH^{\bullet+}$] with different lifetimes, τ.

τ / μs	1	2	5	10	20	50	100
$10^5\sigma$	1.1	8.7	29	44	61	86	104
σ_{rel}♥	1.0	7.9	26.5	40.2	55.8	78.3	95.2
S/*N*♠	90.5	19.6	10.3	9.2	8.5	7.9	7.7

♥ σ_{rel} is the value of σ relative to that when $\tau = 1$ μs.

♠ The signal-to-noise ratio, *S*/*N*, was obtained from *S* = $\max\left[\Phi_S(\theta)\right] - \min\left[\Phi_S(\theta)\right]$ and *N* = σ.

S15. References

1. Frisch MJ*, et al.* (2004) Gaussian 03 (Gaussian, Inc., Wallingford, CT), revision C.02.
2. Rodgers CT (2007) D. Phil. thesis, University of Oxford.
3. Zoltowski BD*, et al.* (2011) Structure of full-length *Drosophila* cryptochrome. *Nature* 480(7377):396-399.
4. Levy C*, et al.* (2013) Updated structure of *Drosophila* cryptochrome. *Nature* 495:E3-E4.
5. Efimova O & Hore PJ (2008) Role of exchange and dipolar interactions in the radical pair model of the avian magnetic compass. *Biophys. J.* 94(5):1565-1574.
6. Müller P, Yamamoto J, Martin R, Iwai S, & Brettel K (2015) Discovery and functional analysis of a 4th electron-transferring tryptophan conserved exclusively in animal cryptochromes and (6-4) photolyases. *Chem. Commun.* 51(85):15502-15505.
7. Timmel CR, Till U, Brocklehurst B, McLauchlan KA, & Hore PJ (1998) Effects of weak magnetic fields on free radical recombination reactions. *Mol. Phys.* 95(1):71-89.
8. Cintolesi F, Ritz T, Kay CWM, Timmel CR, & Hore PJ (2003) Anisotropic recombination of an immobilized photoinduced radical pair in a 50-µT magnetic field: a model avian photomagnetoreceptor. *Chem. Phys.* 294(3):385-399.
9. Till U, Timmel CR, Brocklehurst B, & Hore PJ (1998) The influence of very small magnetic fields on radical recombination reactions in the limit of slow recombination. *Chem. Phys. Lett.* 298(1-3):7-14.
10. Ritz T, Adem S, & Schulten K (2000) A model for photoreceptor-based magnetoreception in birds. *Biophys. J.* 78(2):707-718.
11. Ritz T, Ahmad M, Mouritsen H, Wiltschko R, & Wiltschko W (2010) Photoreceptor-based magnetoreception: optimal design of receptor molecules, cells, and neuronal processing. *J. Roy. Soc. Interface* 7:S135-S146.
12. Lau JCS, Rodgers CT, & Hore PJ (2012) Compass magnetoreception in birds arising from photo-induced radical pairs in rotationally disordered cryptochromes. *J. Roy. Soc. Interface* 9:3329-3337.
13. Solov'yov IA, Mouritsen H, & Schulten K (2010) Acuity of a cryptochrome and vision-based magnetoreception system in birds. *Biophys. J.* 99(1):40-49.
14. Niessner C*, et al.* (2011) Avian ultraviolet/violet cones identified as probable magnetoreceptors. *Plos One* 6(5):e20091.
15. Lau JCS (2013) D. Phil. thesis, University of Oxford.
16. Eriksson LEG & Ehrenberg A (1973) Powder ESR and ENDOR spectra of flavoprotein radicals. *Biochim. Biophys. Acta* 295(1):57-66.
17. Martinez JI, Alonso PJ, & Medina M (2012) The electronic structure of the neutral isoalloxazine semiquinone within *Anabaena* flavodoxin: New insights from HYSCORE experiments. *J. Magn. Reson.* 218:153-162.
18. Martinez JI, Alonso PJ, Gomez-Moreno C, & Medina M (1997) One- and two-dimensional ESEEM spectroscopy of flavoproteins. *Biochemistry* 36(49):15526-15537.
19. Barquera B*, et al.* (2003) X- and W-band EPR and Q-band ENDOR studies of the flavin radical in the Na^+-translocating NADH : quinone oxidoreductase from *Vibrio cholerae*. *J. Am. Chem. Soc.* 125(1):265-275.
20. Weber S, Mobius K, Richter G, & Kay CWM (2001) The electronic structure of the flavin cofactor in DNA photolyase. *J. Am. Chem. Soc.* 123(16):3790-3798.